EXPERIMENTAL INVESTIGATION OF DROPSHAFT HYDRAULICS: TWO-PHASE FLOW AND ACOUSTICS

Hubert CHANSON
Dept of Civil Engineering, The University of Queensland, Brisbane QLD 4072, Australia
Ph.: (61 7) 33 65 43 63 - Fax: (61 7) 33 65 45 99 - E-mail: h.chanson@mailbox.uq.edu.au

Abstract : A dropshaft is an energy dissipator connecting two channels with different invert elevations. Detailed air-water flow and acoustic measurements were conducted in a prototype dropshaft under controlled flow conditions, and complemented by a 1:3.1 scale model study. Experimental observations showed three flow regimes with distinct acoustic signatures. Strong flow aeration was recorded in two flow regimes. Differences between model and prototype results document some limitation of a Froude similitude for studies of air entrainment, residence times and mass transfer in dropshaft.

Keywords : dropshaft, hydraulics, air entrainment, acoustics, physical modelling

INTRODUCTION

A dropshaft is an energy dissipator connecting two channels with different invert elevations (Fig. 1 and 2). This type of structure is commonly used in sewers and storm water systems (e.g. MERLEIN et al. 2002). Small dropshafts are also used upstream and downstream of culverts. The dropshaft is an ancient design and some Roman aqueducts included series of dropshafts (CHANSON 2002a). There is however some controversy if they were used solely for energy dissipation or in combination with flow re-aeration. Despite such long usage, the hydraulics of dropshafts has not been systematically documented : e.g., APELT (1984), RAJARATNAM et al. (1997), MERLEIN et al. (2002).

It is the purpose of this paper to detail the hydraulics and aeration properties of a dropshaft design. New air-water flow and acoustic measurements were performed with a near-full-scale facility (Table 1). The results provide an unique characterisation of the two-phase flow properties in the shaft, including acoustics and particle residence times.

EXPERIMENTAL FACILITIES

A dropshaft design was studied in two flumes (Table 1, Fig. 1). The shafts were built in marine plywood and perspex with a vertical rectangular cross-section. They were designed to be geometrically similar (scaling ratio: 3.1) based upon a Froude similitude with undistorted scale. Similar experiments were conducted for identical inflow conditions d_c/h where d_c is the critical depth in the inflow channel and h is the vertical drop in invert elevation. Further information were reported in CHANSON (2002b).

The discharges were deduced from brink depth measurements and with bend meters calibrated in-situ. Free-surface elevations were recorded with pointer gauges. The total head was measured with a total head tube. Air-water flow properties were measured with a single-tip conductivity probe scanned at 5 kHz for three minutes. Raw probe outputs were recorded at 20 kHz for 10 seconds to calculate bubble chord time distributions. Underwater acoustics were measured with an industrial hydrophone Dolphin Ear™ for fifteen minutes. The signal was digitised with a SoundBlaster 16 card sampled at 40,100 Hz and processed by a bubble-acoustic software StreamTone™ (MANASSEH et al. 2001).

Data processing

The air concentration C is the proportion of time that the probe tip is in the air. The bubble chord time is defined as the time spent by the bubble on the probe tip. Bubble chord times were calculated from the raw probe signal at six different locations per cross-section selected next to the location of maximum void fraction and maximum bubble frequency. The chord time results are presented in terms of pseudo-bubble chord length ch_{ab} defined as :

$$ch_{ab} = V_i \, t_{ch} \quad (1)$$

where V_i is the jet impingement velocity and t_{ch} is the bubble chord time. Equation (1) predicts the exact shape of bubble size probability distribution functions although it overestimates the bubble chord lengths by about 10 to 30% (CHANSON et al. 2002). The acoustic data were analysed using a discrete, pulse-wise analysis. The technique can give good accuracy on the true bubble frequencies, but the conversion to bubble size spectra relies upon the questionable assumptions that bubbles of different sizes are perturbed to the same proportional extent and that the bubble do not interact acoustically.

Table 1 - Experimental investigations of rectangular dropshafts

Ref.	Drop height h m	Pool depth m	Shaft length m	Shaft width m	b_1 m	D_1 ([1]) m	b_2 m	D_2 m	Remark
Present study	1.70	1.00	0.755	0.763	0.50	0.30	0.50	0.30	Prototype (Fig. 1).
	0.548	0.322	0.243	0.246	0.161	0.25	0.209	0.097	Model.
CHANSON (2002a)	0.505	0.365	0.30	0.30	0.144	0.25	0.15	0.25	Recret model.
	0.668	0.201	0.20	0.30	0.110	0.25	0.11	0.21	Valdepuentes (90º turn).
	0.668	0.201	0.20	0.30	0.110	0.25	0.11	0.21	Valdepuentes (180º turn).
APELT (1984)	0.325	0	0.152	0.152	Pipe : Ø = 0.152 m		Pipe : Ø = 0.152 m		

Notes : ([1]) : sidewall height; b : channel breath; D : Channel height; 1 : upstream channel; 2 : downstream channel.

DROPSHAFT HYDRAULICS

The upstream and downstream channels operated as free-surface flow for all investigated flow conditions. The inflow conditions were subcritical, while the outflow channel operated with supercritical flows. Three flow regimes were observed as functions of the flow rate. At low flow rates (i.e. $d_c/h < 0.0038$), the free-falling nappe impacted into the shaft pool (regime R1, Fig. 1). Substantial air bubble entrainment took place in the shaft pool. In the downstream channel, the flow was supercritical and shock waves developed. For intermediate discharges ($0.0038 < d_c/h < 0.0048$), the free-falling nappe impacted into the outflow channel (regime R2). The pool free-surface level increased significantly, almost no air bubble entrainment was observed in the pool and very-large invert pressure fluctuations were observed in the prototype. At large flow rates ($0.0048 < d_c/h$), the free-jet impacted onto the opposite wall above the downstream conduit obvert (regime R3) (Fig. 2). Significant water deflections took place in the shaft associated with substantial air entrainment in the shaft pool.

Residual energy data are presented in Figure 3 as H_2/H_1 as a function of the dimensionless flow rate d_c/h, where H_2 is the downstream residual head and H_1 is the upstream total head

measured above downstream channel invert. Model and prototype results are compared with the data of CHANSON (2002a). Low residual heads, associated with high energy dissipation, were achieved at low flow rates (Regime R1). Poor dissipation performances were observed in regime R2. In regime R3, the dimensionless residual head ranged from 20 to 35% for the investigated flow conditions.

Pool free-surface height data showed an increase in pool height with increasing discharges. The trend was consistent with the data of RAJARATNAM et al. (1997). Visual observations of bubble penetration depths showed substantial aeration in the shaft pool, but in the regime R2. Prototype observations however indicated a lesser bubbly flow volume than in model for identical dimensionless flow rates d_c/h, in both regimes R1 and R3. The finding highlights the limitations of misleading, simplistic visual observations and potential scaling effects.

AIR-WATER FLOW PROPERTIES

Detailed air-water flow measurements were conducted with a sturdy single-tip conductivity in the prototype in regimes R1 and R3. They showed strong flow aeration. Preliminary measurements, conducted at various transverse locations y, indicated that the void fraction distributions were basically two-dimensional, but next to the outer edges of free-falling nappe impact. Typical distributions of centreline void fraction C are presented in Figure 4, where x is the horizontal distance measured from the downstream shaft wall, and z is the vertical direction positive downwards with z = 0 at the pool free-surface. Experimental results (Fig. 4) demonstrated very high void fractions close to the free-surface for all flow conditions : i.e., for z < 50 mm. The large measured void fractions could not be attributed to measurement error. The plunge point region was visually very aerated and it had an appearance somehow similar to a hydraulic jump roller. Further the pool free-surface elevation fluctuated at low frequency with time. It is conceivable that the probe tip was in air for brief periods, although this was not visually observed.

In regime R1, the plunging jet flow was characterised by smooth, derivative profiles of void fractions (Fig. 4). The centreline data illustrated consistently the advective diffusion of entrained air associated with a quasi-exponential decay of maximum air content with longitudinal distance from impingement and a broadening of the air diffusion layer. The data were best fitted by an analytical solution of the diffusion equation for air bubbles :

$$C = \frac{1}{2} \frac{Q_{air}}{Q} \frac{1}{\sqrt{8 \pi D^{\#} \frac{z}{d_i}}} \left(\exp\left(- \frac{1}{2 D^{\#}} \frac{\left(\frac{x - x_i}{d_i} - \frac{1}{2} \right)^2}{\frac{z}{d_i}} \right) + \exp\left(- \frac{1}{2 D^{\#}} \frac{\left(\frac{x - x_i}{d_i} + \frac{1}{2} \right)^2}{\frac{z}{d_i}} \right) \right)$$

Two-dimensional free-falling plunging jet (2)

where Q_{air} is the volume air flow rate, d_i is the thickness of the free-jet at impact and x_i is the jet impact coordinate, and $D^{\#}$ is a dimensionless air bubble diffusivity. Equation (2) is shown in Figure 4, where the values of $D^{\#}$ and Q_{air}/Q were determined from the best fit of the data. Note that the data were measured in the fully-developed flow region (i.e. $z/d_i > 10$).

PARTICLE RESIDENCE TIMES AND BUBBLE SIZE DISTRIBUTIONS

Residence times in the shaft pool were recorded using neutrally-buoyant particles. Initial tests showed that the data were basically independent of particle sizes (3.3 to 9 mm in model, 5 to

15 mm in prototype) for all flow regimes and configurations. Typical probability distribution functions of dimensionless residence times are presented in Fig. 5. In regime R1, the particle residence times was comparatively the greatest (Fig. 5). In regime R2, the free-falling nappe flowed directly into the outflow channel. Most particles were directly entrained into the outflow conduit, corresponding to a very-small residence time. In regime R3, particles were sometimes entrained down the shaft pool but most exited the shaft rapidly. The same trends were observed in both model and prototype, although some quantitative differences were noted (Fig. 5).

In regime R1, the residence time probability distributions exhibited a distinctive bi-modal shape. About 45% of the particles flowed downwards at nappe impact and were entrained rapidly into the outflow channel (Mode 1). For the data shown in Figure 5, the first mode is centred around T^*V_c/d_c = 66 and 33 for model and prototype respectively. The rest of particles (i.e. 55%) were trapped in large scale vortices (Mode 2), sometimes passing from one structure to another, until they were finally entrained in the downstream conduit. Mode 2 data are centred roughly around T^*V_c/d_c = 1770 and 1230 for model and prototype respectively. These values may be compared with the average filling time of the shaft pool of about T^*V_c/d_c = 770.

Pseudo-chord size distributions

Pseudo-bubble chord length distributions are presented in Figure 6, showing the normalised probability distribution function of pseudo air chord length ch_{ab} where the histogram columns represent the probability of chord length in 0.5 mm intervals. The last column (i.e. > 15) indicates the probability of chord lengths exceeding 15 mm. Each histogram describes the bubbles detected in a cross-section at depths z = 30, 150 and 250 mm.

For all flow conditions (regimes R1, R2 and R3), the data demonstrated a broad spectrum of pseudo-bubble chord lengths at each cross-section : i.e., from less than 0.5 mm to larger than 15 mm (Fig. 6). The pseudo-bubble chord length distributions were skewed with a preponderance of small bubble sizes relative to the mean. The probability of bubble chord length was the largest for bubble sizes between 0 and 2 mm although the mean pseudo-chord size was between 10 and 20 mm. The data were possibly best fitted by a log-normal distribution, although both Gamma and Weibull distributions provided also good fit. The results were consistent with experimental measurements in the developing flow region of vertical plunging jets (CUMMINGS and CHANSON 1997, CHANSON et al. 2002).

ACOUSTICS PROPERTIES

Prototype acoustic spectra were measured for several jet velocities corresponding to the three flow regimes (CHANSON 2002b). In first approximation, the bubble diameter is inversely proportional to the sound frequency : i.e., small bubbles generate high-frequency sound. Each acoustic spectrum showed a minimum in energy at roughly 200-400 Hz, indicating that low-frequency noise due to background turbulence is below 400 Hz. The aliasing frequency of the equipment of 22 kHz. Since the peaks fall off well before 3 kHz, it is believed that they are genuine acoustic properties, subject only to the uncertainties of the assumptions in the analysis.

The analysis of acoustic spectra showed marked differences between each flow regime. In regime R1, the acoustic signature showed a broad, flat curve between F = 0.5 and 1.6 kHz, corresponding to bubbles about 4 to 12 mm in diameter. In Regime R2, there was a definite

peak at about F = 1.7 kHz, corresponding to bubbles about 3.8 mm in diameter. In Regime R3, the spectrum had a flat curve between F = 0.5 and 1 kHz. The acoustic signatures of the shaft bubbly flow characterised clearly the change in flow regimes visually observed. An identical result was obtained with a lower, cruder sampling rate. The result suggests that an acoustic technique, calibrated through detailed laboratory measurements, may provide useful insights in dropshaft operation where the robust sensor can be used in hostile conditions.

SUMMARY AND CONCLUSION

Detailed air-water flow and acoustic measurements were conducted in a prototype dropshaft under controlled flow conditions. The study was complemented by a 1:3.1 scale model study. Experimental observations showed three basic flow regimes. The rate of energy dissipation was nearly 95% at low flow rates (Regime 1). In that flow regime, probability distribution functions of particle residence times exhibited a bi-modal distribution. Some particles plunged into the shaft pool and rapidly exited into the outflow conduit. Others remained trapped in large-scale vortical structures for up to 20 minutes. Void fraction measurements demonstrated a strong aeration of the shaft pool for all flow regimes, but regime R2. For low flow rates, void fraction distributions were successively compared with an analytical solution of the air bubble advective diffusion equation. Acoustic signatures of the bubbly flow characterised accurately the changes in flow regimes.

Although basic hydraulic characteristics were similar between model and prototype based upon a Froude similitude, observations of dimensionless bubble penetration depths and neutrally-buoyant particle residence times showed some discrepancy between model and prototype results. It is believed that these differences highlight the limitations of a Froude similitude for studies of air entrainment, residence times and mass transfer in dropshaft.

ACKNOWLEDGMENTS

The writer thanks his students Joel I. WILSON and Craig RUSSELL who collected the data, Dr Richard MANASSEH (CSIRO Melbourne) for valuable advice, and G. ILLIDGE and B. McPHAIL.

REFERENCES

APELT, C.J. (1984). "Goonyella Railway Duplication Drop Structures and Energy Dissipators at Culvert Outlets. Model Studies." *Report CH27/84*, Dept of Civil Eng., Univ. of Queensland, Brisbane, Australia, Feb., 10 pages, 11 figures & 37 plates.

CHANSON, H. (2002a). "An Experimental Study of Roman Dropshaft Hydraulics." *Jl of Hyd. Res.*, IAHR, Vol. 40, No. 1, pp. 3-12.

CHANSON, H. (2002b). "An Experimental Study of Roman Dropshaft Operation : Hydraulics, Two-Phase Flow, Acoustics." Report CH50/02, Dept of Civil Eng., Univ. of Queensland, Brisbane, Australia.

CHANSON, H., AOKI, S., and HOQUE, A. (2002). "Similitude of Air Bubble Entrainment and Dispersion in Vertical Circular Plunging Jet Flows. An Experimental Study with Freshwater, Salty Freshwater and Seawater." *Coastal/Ocean Engineering Report*, No. COE02-1, Dept. of Architecture and Civil Eng., Toyohashi University of Technology, Japan, 94 pages.

CUMMINGS, P.D., and CHANSON, H. (1997). "Air Entrainment in the Developing Flow Region of Plunging Jets. Part 2: Experimental." *Jl of Fluids Eng.*, Trans. ASME, Vol. 119, No. 3, pp. 603-608.

MANASSEH, R., LAFONTAINE, R. F., DAVY, J., SHEPERD, I. C., and ZHU, Y. (2001). "Passive Acoustic Bubble Sizing in Sparged Systems." *Experiments in Fluids*, Vol. 30, No. 6, pp. 672-682.

MERLEIN, J., KLEINSCHROTH, A., and VALENTIN, F. (2002). "Systematisierung von Absturzbauwerken." *Mitterilung No. 69*, Lehrstuhls fur Hydraulik und Gewasserkunde, Technishen Universitat Munchen, Germany, 206 pages.

RAJARATNAM, N., MAINALI, A., and HSUNG, C.Y. (1997). "Observations on Flow in Vertical Dropshafts in Urban Drainage Systems." *Jl of Environmental Engrg.*, ASCE, Vol. 123, No. 5, pp. 486-491.

Fig. 1 - Dropshaft definition sketch
Regime R1- Prototype dimensions

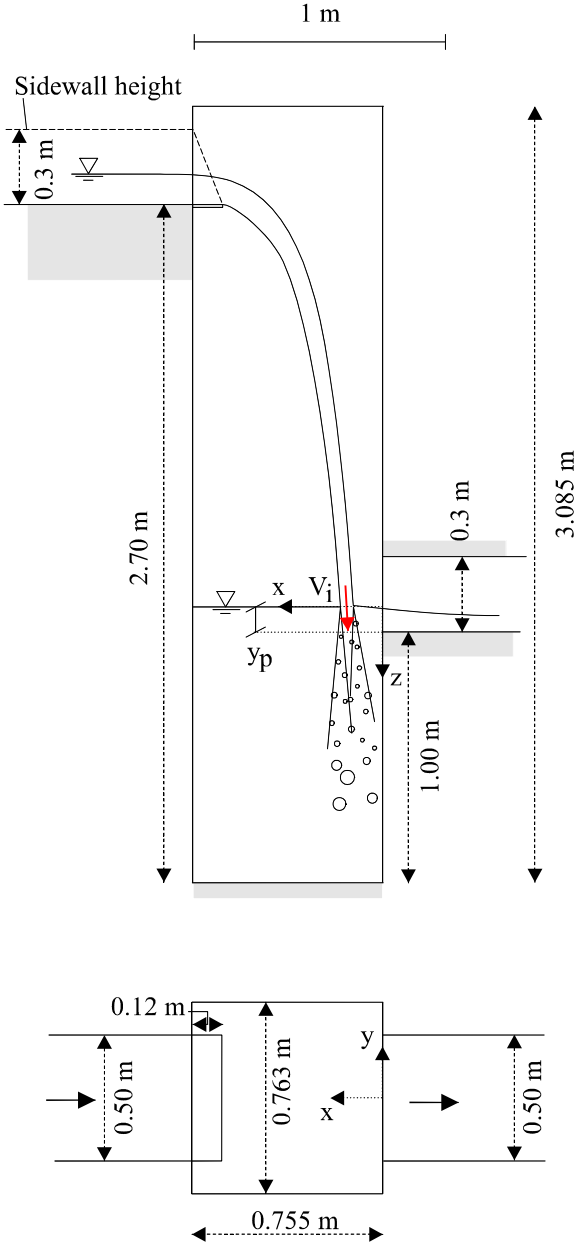

Fig. 2 - Dropshaft operation (prototype)
Regime R3, Q = 0.067 m^3/s - Flow from top right to bottom left

Fig. 3 - Dimensionless residual head H_2/H_1 as function of the dimensionless flow rate d_c/h - Comparison with CHANSON's (2002a) data

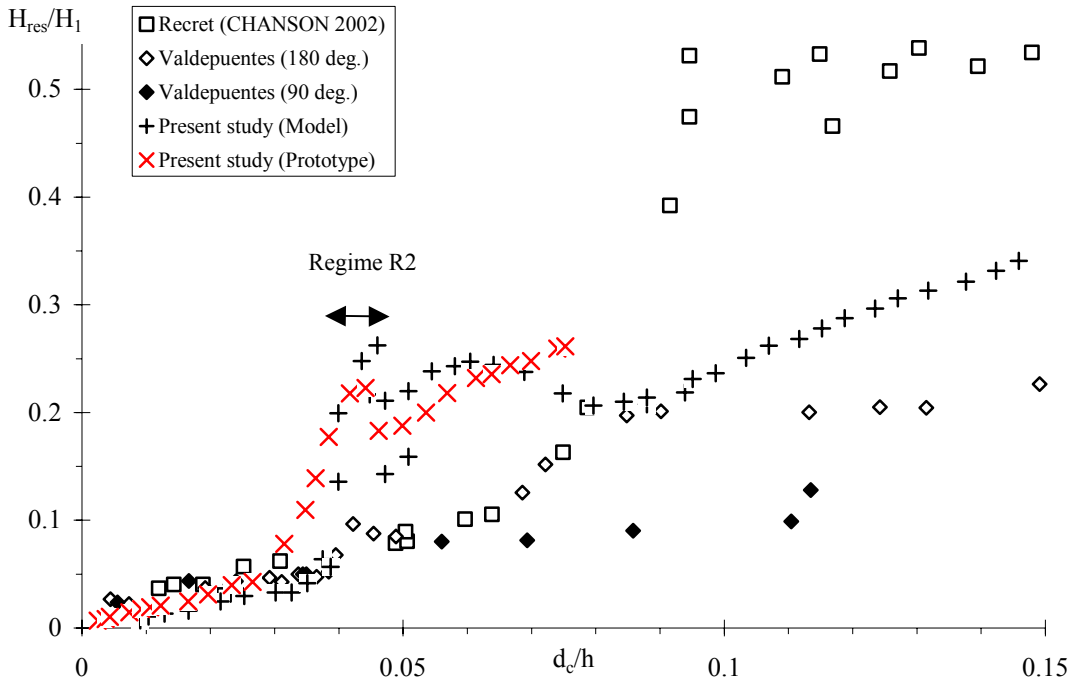

Fig. 4 - Air concentration distributions beneath the pool free-surface on the shaft centreline - Prototype data for $d_c/h = 0.017$ (Regime R1) - Comparison with Equation (2)

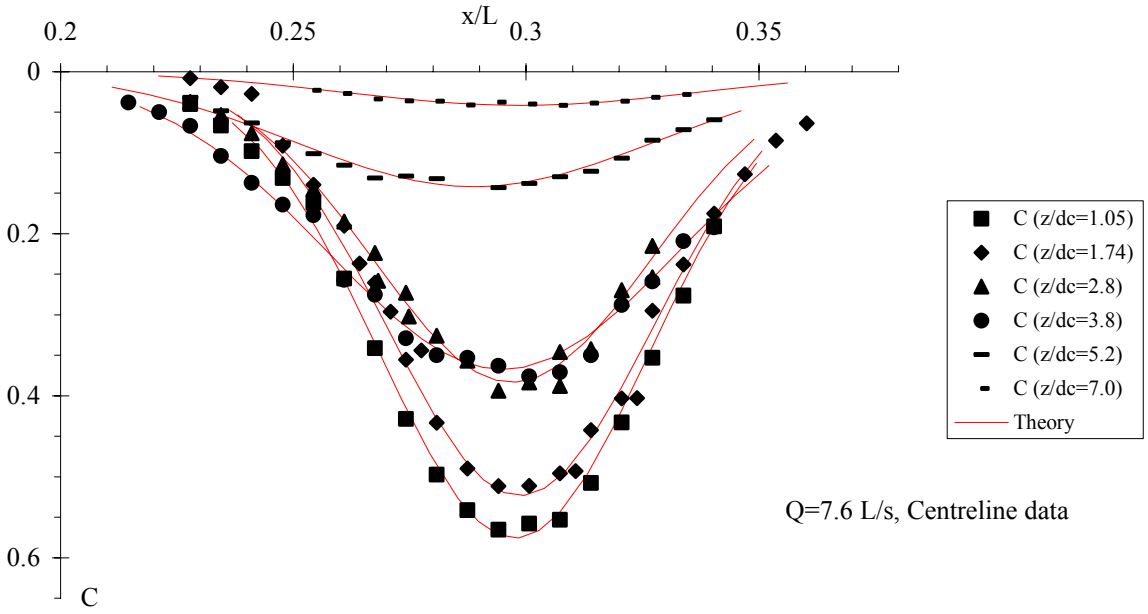

Fig. 5 - Probability distribution functions of dimensionless residence time T_R*V_c/d_c (prototype and model data)

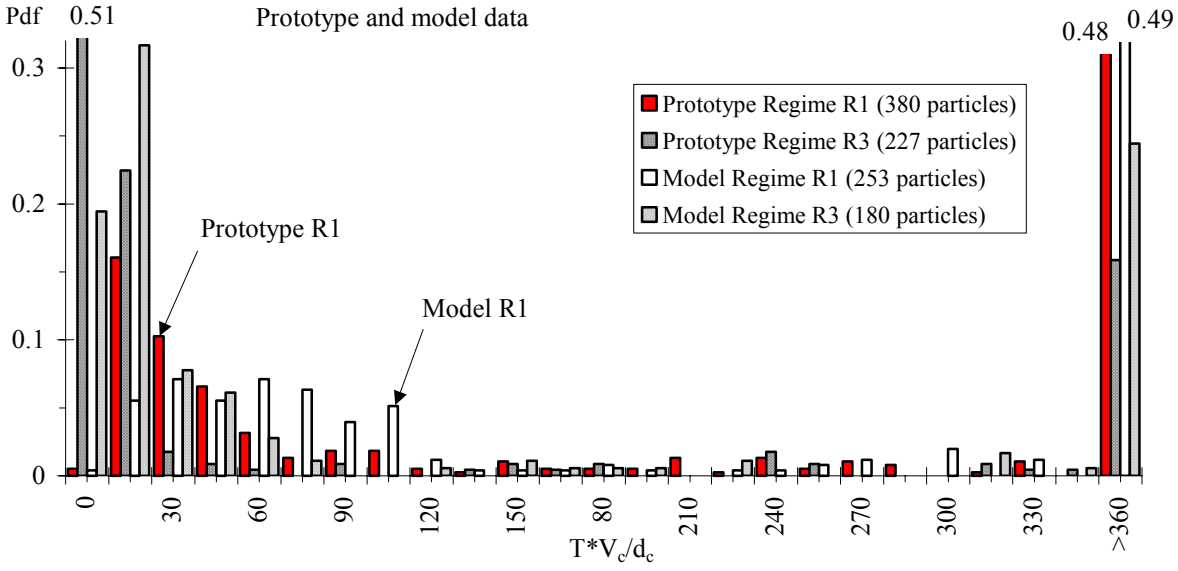

Fig. 6 - Probability distribution functions of pseudo air chord sizes in Regime R3 - Prototype data, Q = 0.067 m^3/s, d_c/h = 0.072 (centreline data)